Design and Control of a Cable-Driven Articulated Modular Snake Robot

Peter Racioppo, *Student Member, IEEE*, and Pinhas Ben-Tzvi, *Senior Member, IEEE*

***Abstract*—This paper presents the design and control of a cable-actuated mobile snake robot composed of modular coupled linkages. The goal of this research is to reduce the size of snake robots and improve their locomotive efficiency by simultaneously actuating groups of links to fit optimized curvature profiles. The basic functional unit of the snake is a four-link, single degree of freedom module that bends using an antagonistic cable-routing scheme. The mechanical and electrical designs of the module are first presented, with emphasis on the cable-routing scheme, key optimizations, and the use of elastic elements. A simplified model of serpentine locomotion is then presented and used to derive some properties of this locomotion gait. Control strategies for snake robots with coupled joints are also developed, including a feedback linearization of the pulley dynamics using the coupled cable equations. Experiments using a fully integrated prototype are presented and compared with simulated results.**

***Index Terms*—Force control, mobile robots, modeling, robot dynamics, snake robot.**

I. Introduction

SNAKE ROBOTS, like their biological counterparts, consist of serial-linkages, and locomote primarily by pushing against external objects using undulatory waves [1]. These robots are typically highly articulated, allowing them to change their body shape to manipulate external objects and operate in a wide variety of environments [2]. The lateral undulation gait, more commonly called serpentine or slithering locomotion, allows a snake to generate propulsive forces by propagating sinusoidal waves along its length, provided that it makes anisotropic frictional contact with the ground, with higher coefficients of friction normal to its body length than along it body length [3], [4]. Unlike wheeled or legged robots, a snake robot may thus engage any part of its body to locomote, making it well suited to cluttered or confined spaces likely to be encountered in, e.g., search and rescue missions or inspection tasks [5]. Undulatory locomotion is also a notably energy-efficient and silent means of transportation, and is thus appropriate for use in a variety of prolonged or covert activities [4]. Snakelike robots have also found use as manipulators, including in surgical settings, where their ability to conform to narrow channels such as the throat and ear canal make them well suited for use as surgical instruments [6], [7].

Modern mobile snake robots typically feature about an order of magnitude fewer joints per length than biological snakes [8], and rely on individual motors to drive each joint, in contrast to the complex web of musculature used in nature. Direct drive mechanisms have been used in a wide variety of these robots, including the first snake robot ACM III [9]; the robots developed in [10] and [11], which demonstrated pole climbing and obstacle traversal; snakes with active wheels or treads such as the ACM-R4.1 and OmniTread OT-8, [12], [13]; and the modular self-reconfigurable MTRAN and PolyBot robots [14], [15]. With fewer joints per length than biological snakes, robotic snakes must drive their joints at greater amplitude to approximate a given curvature profile, and are limited by the mass and cross-sectional area requirements of their actuators. Snakelike manipulators have achieved smaller cross section than mobile snake robots through the use of axially routed cables, which allow actuators to be located away from the joints of the end-effector. Notable examples include the CardioARM robot, intended for heart surgery, which features cylindrical links of only 10-mm diameter actuated by internally routed cables [6], and the continuum manipulator of Ouyang *et al*. [16], which consists of a three-segment, super-elastic nitinol rod backbone actuated by axial cables. These systems achieve extremely small scale and high articulation, but require external pulleys and actuators, and thus are not suited for use in mobile robots. To address these issues, we have developed a multilink mechanism that can simultaneously actuate a group of four links using agonist-antagonist cable pairs routed around a multiradius pulley. The modular design of this mechanism is intended to support two design paradigms, either serving as the basic functional unit in a highly articulated snake robot or allowing snake robots with fewer degrees of freedom (DOFs) to respond passively to obstacles.

The work presented in this paper is part of ongoing research on the design and control of snakelike robots [17], [18], and of cable-actuated mechanisms with continuum [19], [20] and serpentine [21] structures. This paper is organized as follows: Section II presents the mechanical and electrical design of the

Manuscript received July 18, 2018; revised January 28, 2019; accepted March 16, 2019. Date of publication March 19, 2019; date of current version June 14, 2019. Recommended by Technical Editor T. Seo. *(Corresponding author: Pinhas Ben-Tzvi.)*

P. Racioppo was with the Robotics and Mechatronics Laboratory, Mechanical Engineering Department, Virginia Tech, Blacksburg, VA 24061 USA. He is now with the University of California, Los Angeles (UCLA), Los Angeles, CA, USA (e-mail: pcracioppo@gmail.com).

P. Ben-Tzvi is with the Robotics and Mechatronics Laboratory, Mechanical Engineering Department, Virginia Tech, Blacksburg, VA 24061 USA (e-mail: bentzvi@vt.edu).

Color versions of one or more of the figures in this paper are available online at http://ieeexplore.ieee.org.

Digital Object Identifier 10.1109/TMECH.2019.2906298

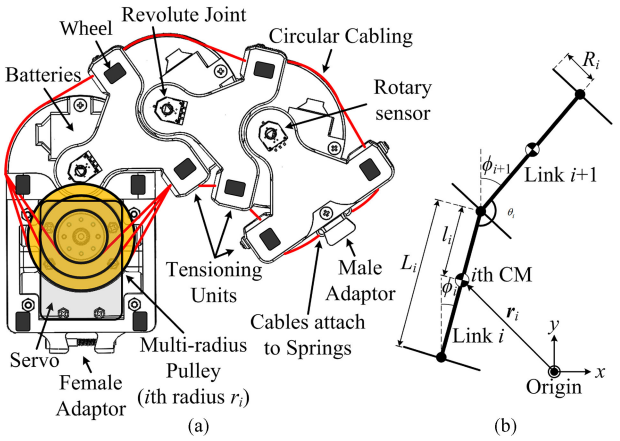

Fig. 1. (a) Mechanical design of a four-link module near full extension. (b) Definitions of coordinates and design parameters.

snake robot. Section III discusses a simplified "single-body model" of lateral undulation. Section IV develops a control scheme for the robot. Section V presents experiments on locomotion and obstacle interaction using a two-module prototype. Concluding remarks and plans for future work are discussed in Section VI.

II. Design

This section presents the design of the snake robot, including the cable-routing scheme and design synthesis of a single module, and then outlining the electronic design and implementation of a preliminary two-module prototype.

A. Mechanical Design

Each module, as pictured in Fig. 1(a), is a single-DOF unit, composed of a serial chain of four rigid links connected by parallel revolute joints. The mechanism is actuated by three pairs of antagonistic cables, each of which is routed along circular grooves on the link exteriors rather than axially, constraining the cable displacements in agonist-pairs to be approximately equal and opposite in value. Each cable is wound around a section of a multiradius pulley and attaches to an extension spring on a single link, passing through sliding tensioning units in intermediate links, which keep the cables from slipping normal to the links and prevent backlash and hysteresis-nonlinearities. Attached to the bottom of each link are two 2.5-cm diameter, plastic wheels oriented parallel to the length of the snake, giving the robot's bottom surface orientation-dependent friction coefficients that are close to ideal for planar locomotion. Modules connect serially via a rigid male–female interface.

Link cross section is constrained by the dimensions of the pulley and actuator, and minimizing cross section must be traded off with maximizing the number of links in a module. Link lengths are set as the minimum necessary to accommodate rotation about semicircular surfaces with diameters equal to the width of the links. Minimizing the length to width ratio of the links is also necessary to minimize differences in the antagonistic cable displacements [17]. The arc of the link surfaces is chosen as 180° in order to maximize the maximum angle that can be achieved before antagonistic cable displacements become unequal. With the above-mentioned optimizations, the mechanism achieves less than 0.4% simulated difference in all antagonistic cable displacements at joint angular displacements of up to 35° [17].

Assuming zero spring extension, rotating the multiradius pulley by an angle θ_P induces a curvature profile in the mechanism, given in terms of the angular position of the ith joint θ_i (where $i = 1$ at the actuation link), by

$$\theta_i \approx \left(\frac{r_i}{R_i} - \frac{r_{i-1}}{R_{i-1}} \right) \theta_P . \tag{1}$$

As illustrated in Fig. 1(b), r_i is defined as the ith pulley radius, R_i is the radius of the ith semicircular link, and L_i is the distance between the (i–1)th and ith joints. The pulley radii can thus be chosen so that the linkage fits a particular convex curvature profile at a given pulley angular displacement. We discuss an optimization procedure for the case of a snake robot in Section IV. Given the motor and pulley constraints, link dimensions were chosen as $L = 50$ mm and $R = 35$ mm, and the optimized pulley radii were computed as $r_1 = 8.5$ mm, $r_2 = 16$ mm, and $r_3 = 22.5$ mm, permitting maximum angular displacements of 55°, 48.5°, and 42° at joints one, two, and three, respectively.

The multiradius pulley is rotated with a high-torque servomotor equipped with a rotary encoder, which, using the kinematic constraints in (1), is sufficient to measure the full body-shape of the module, provided that the springs are unextended. Rotary position sensors located at each joint measure spring displacements, for use in the obstacle interaction procedure described in Section IV. The ith joint torque τ_i of an N-link linkage due to a motor torque τ_M can be computed by solving recursively from the end of the mechanism to its base, and are given in terms of the $N-1$ agonist cable forces F_i by a set of N equations [17]

$$\tau_M = \sum_{i=1}^{N-1} F_i r_i, \quad \tau_i = \sum_{j=1}^{N-1} F_j R_j . \tag{2}$$

B. Elastic Elements

Elastic elements are commonly used in robotics applications as a means of low-pass filtering impacts, storing energy during locomotion, and enabling force control by mapping displacements to forces [22]. In snake robots, previous work includes the development of a torsional rubber series elastic actuator by Rollinson *et al.* [23], [24], for use in a pole-climbing snake robot. In this section, we consider the use of extension springs placed in series with each cable. Extension springs are smaller and easier to implement than specialized torsional springs and are well suited to a cable transmission system. Spring constants of approximately 500 N/m were selected to permit desired angular displacements under anticipated contact forces. At the servomotor's stall torque, the springs allow up to 12° of joint rotation, enough to significantly alter the robot's shape. With an effective torsional spring constant of 17.5 N/m/rad, this spring-cable system produces joint stiffness comparable to the torsional SEAs employed in [24].

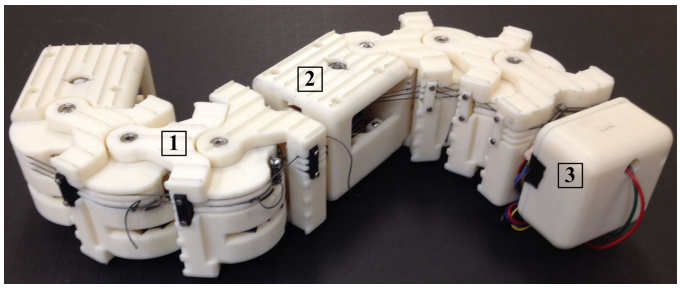

Fig. 2. Two-module snake robot prototype, showing (1) a semicircular link, (2) actuation link with servomotor, and (3) control module with MCU/IMU.

With the addition of springs, the cable constraints give rise to coupled joint rotation in the presence of external forces. During unimpeded motion, displacements in antagonistic cables are equal and opposite, so the springs are not engaged. However, spring displacements in agonist cables induced by external forces will cause spring displacements in the antagonist cables at subsequent links, since no extra cable length has been provided for them, causing the mechanism to passively bend toward the force. If each of the i joints between joints n through m are forcibly displaced by an angle ε_i, the $(m+1)$th link must rotate to compensate for their rotation

$$\sum_{i=n}^{m} \varepsilon_i = -\sum_{j=m+1}^{N} \varepsilon_j . \tag{3}$$

C. Electrical Design

The robot is powered by two 600-mAh, 3.7-V lithium polymer batteries per link, or by a single external power cord. The batteries are wired in series along the module's central axis, and power the servomotor, rotary sensors, and an ARM Cortex M4 microcontroller. Each pulley is actuated with an RX-28 servomotor. Each servomotor features an inbuilt MAX485 driving chip and an angular encoder with 0.29° resolution. The robot receives high-level steering commands from a PC-based user interface, using 2.4-GHz radio frequency transceiver modules. A small "control module" carries the microcontroller and supporting electronics as well as a nine-axis inertial measurement unit (IMU), which acquires magnetic orientation, angular rates, and acceleration data at a 200-Hz update rate and transmits to the MCU via an I^2C bus. Analog rotary position sensors located at each joint relay joint angular displacement data to the MCU. Measurements when the robot is not encountering obstacles are used to calibrate the kinematic constraint constants in (1). The fully integrated prototype, pictured in Fig. 2, measures 53 cm × 7 cm × 7 cm at full extension, with a mass of 1.53 kg.

III. Dynamic Modeling

This section begins by presenting background on the lateral undulation gait, the most common and most efficient method of locomotion used by biological snakes [5], [25]. We then introduce a simplified model of this gait and compare its predictions with those of a detailed multibody dynamic (MBD) model.

A. Lateral Undulation

The approximate body shape of a biological snake performing lateral undulation can be approximated by the so-called "serpenoid curve," first described by S. Hirose [1]. A snake robot with N identical links and uncoupled joints can form a discrete approximation to a serpenoid curve by driving each of its $i \in [1, N-1]$ joints to track

$$\theta_{\mathrm{ref},i} = \alpha \sin\left(\omega t + (i-1)\,\delta\right) + \theta_0 \tag{4}$$

where α is the maximum joint angular displacement, ω is the angular frequency, δ is a phase offset that affects the efficiency of locomotion, and θ_0 is a heading offset that induces approximately constant-curvature turning for constant, nonzero values [26].

Liljebäck *et al.* [5] showed that the δ that maximizes the speed of a snake robot following (4) in a simplified dynamic model can be approximated by the δ that maximizes $k_\delta \equiv \sum_{i=1}^{N-1}\sum_{j=1}^{N-1} c_{ij}\sin((j-i)\delta)$ where c_{ij} is the ijth element of $\mathbf{C} = \mathbf{A}\mathbf{D}^T(\mathbf{D}\mathbf{D}^T)^{-1} \in \mathbb{R}^{(N-1)\times(N-1)}$, with

$$\left\{ \mathbf{A} = \begin{bmatrix} 1 & 1 & \cdots & 0 \\ \vdots & \ddots & & \vdots \\ 0 & \cdots & 1 & 1 \end{bmatrix}, \mathbf{D} = \begin{bmatrix} 1 & -1 & \cdots & 0 \\ \vdots & & \ddots & \vdots \\ 0 & & \cdots & -1 \end{bmatrix} \right\} \in \mathbb{R}^{(N-1)\times N}.$$

We obtain a closed-form approximation for $\bar{\delta}(N)$, the optimal value of δ as a function of N, by deriving a property of $\mathbf{C}$. For brevity, we give only a sketch of the proof here.[1] First, let $n \equiv N-1$ and $\mathbf{B} \equiv (\mathbf{D}\mathbf{D}^T)^{-1} \in \mathbb{R}^{n\times n}$, to simplify the notation. It can be shown that the sum of the kth diagonal of $\mathbf{B}$ is $b_k = \frac{T_k}{n+1}$ where T_k is the kth tetrahedral number $T_k = k(k+1)(k+2)/6$. (By the kth diagonal, we mean counting from the bottom left or top right corner of a matrix and moving toward the main diagonal.) It follows that the off diagonals of $\mathbf{C}$ sum to $c_k = \frac{\pm 2t_k}{n+1}$ where t_k is the kth triangular number $t_k k(k+1)/2$ and where the plus sign corresponds to the upper triangle of the matrix and the minus sign to the lower triangle. Given the previous fact about $\mathbf{C}$, the above-mentioned double sum expression for k_δ can be reduced to a single sum: $k_\delta = \frac{2}{N}\sum_{k=1}^{N-1} k(k+1)\sin((N-1-k)\delta)$.

Expanding k_δ and setting the derivative equal to zero

$$\frac{1+N(N-1)}{N+1}\cos\left(\bar{\delta}\right) + \frac{N-2}{N+1}\cos\left(\bar{\delta}N\right) = \cos\left(\bar{\delta}\,(N-1)\right) N - 2\,.$$

Taylor expanding to fourth order at $\bar{\delta} = 0$, then taking two terms in the Taylor expansion at $N = \infty$ and rounding to the hundredths place gives

$$\bar{\delta} \approx \frac{4.10}{N} + \frac{2.15}{N^2}. \tag{5}$$

This expression approximates the original formulation (defined by k_δ) to 2.75% error for all $3 \le N \le 100$.

[1] A full version can be found at the RML GitHub page: https://github.com/RM-Lab/Robosnake/blob/master/Supplements.pdf

B. Single-Body Model of Lateral Undulation

This section presents a simplified model of lateral undulation that attempts to approximate the detailed dynamics of this gait by considering the forces acting on an individual link as it moves through a sinusoidal trajectory. We consider a snake with N links of uniform length L and mass m undergoing lateral undulation in the xy plane, with global coordinates $\mathbf{r}_i = [x_i\ y_i]^{\mathrm{T}}$. Taking the snake's heading to be in the y-direction, the acceleration of its ith link due to anisotropic viscous friction is

$$\ddot{\boldsymbol{r}}_i = -\frac{1}{m}\mathbf{R}_i^T \boldsymbol{\Omega}_i \mathbf{R}_i \dot{\boldsymbol{r}}_i \tag{6}$$

where $\boldsymbol{\Omega}_i = \mathrm{diag}(c_{n,i},\, c_{t,i})$ is a diagonal matrix of the normal and transverse coefficients of friction, respectively, and $\mathbf{R}_i$ is the rotation matrix corresponding to a rotation about the z-axis by an angle ϕ_i. Here, $\phi_i = a\sin(\omega t + (i-1)\delta)$ is the ith link's global orientation, as it oscillates sinusoidally with amplitude a. The terms on the main diagonal in (6) correspond to braking forces and those on the off diagonal to propulsive forces [5]. We here consider the case that the snake is traveling with low period-averaged acceleration and low amplitude a, and closely follows the serpenoid curve, with $\delta \approx \bar{\delta}$.

Without loss of generality, define link k as having orientation $\phi_k = 0$ at $t = 0$, such that $\phi_k = a\sin(\omega t)$. The maximum lateral displacement of a snake moving along the y-axis is half the distance between subsequent links of orientation zero, which is half the sum of the projections onto the x-axis of links k through m where m is given by the constraint equation $\sum_{i=0}^{2m}\sin(i\delta) = \sum_{i=0}^{2m-1}\sin(i\delta) = 0$. It follows that $m = \pi/\delta$, and the x-displacement of link k, provided that $a \ll 1$, is then

$$x_k = -\frac{L}{2}\sum_{i=1}^{\pi/\delta}\sin\left[a\sin\left(\omega t + i\delta\right)\right] \approx -\frac{La}{2}\sum_{i=1}^{\pi/\delta}\sin\left(\omega t + i\delta\right).$$

Expanding the summation and differentiating

$$\dot{x}_k \approx \frac{La\omega}{2}\csc\left(\frac{\delta}{2}\right)\sin\left(\omega t + \frac{\delta}{2}\right). \tag{7}$$

Since, by construction, the snake's period-averaged velocity is approximately constant and $\theta_0 \approx 0$, each link traces out nearly the same path [1], and must thus contribute approximately equally over an oscillation period to propulsive and drag forces.

Substituting (7) into the upper right component of (6), the y-component of the snake's period-averaged propulsive force at $\delta \approx \bar{\delta}$, normalized by its body length, is given by the integral

$$\bar{F}_p \approx \frac{a\omega^2\left(c_n - c_t\right)\csc\left(\frac{\bar{\delta}}{2}\right)}{4\pi N}\int_0^{2\pi/\omega} \sin\left(\phi_k\right)\cos\left(\phi_k\right)\sin\left(\omega t + \frac{\bar{\delta}}{2}\right)dt.$$

By (5)

$$\bar{F}_p\left(N\right) \approx \frac{J_1\left(2\right)}{2}\left(a\omega\right)^2\left(c_n - c_t\right)\frac{1}{N}\cot\left(\frac{2.05}{N} + \frac{1.08}{N^2}\right) \tag{8}$$

where $J_n(z)$ is the Bessel function of the first kind. Thus, as the number of links comprising the snake increases, its period-average propulsive force increases monotonically, by approximately 51.5% from $N = 3$ to $N = \infty$.

The angular dynamics of link k may be written as: $I\ddot{\phi}(t) = \tau_u(t) - f_v\dot{\phi}(t) + f_i(\phi(t), \dot{\phi}(t))$ where the constant $f_v = \lim_{n\to\infty}\frac{2c_n l^2}{n}\sum_{i=0}^{n}\left(\frac{i}{n}\right)^2 = \frac{2}{3}c_n\left(\frac{L}{2}\right)^2$ accounts for frictional braking due to rotation of a link of constant mass density, $\tau_u(t) = k_p[\alpha\sin(\omega t) - \phi(t)] + k_d[\alpha\omega\cos(\omega t) - \dot{\phi}(t)]$ is a PD control torque (where k_p and k_d are gains), and f_i is the angular component of the generalized forces internal to the mechanism. For simplicity, f_i and f_v can be eliminated by a partial feedback linearization of the joint dynamics [5], giving $I\ddot{\phi}(t) = [k_p\alpha\sin(\omega t) + k_d\alpha\omega\cos(\omega t)] - b\phi(t) - c\dot{\phi}(t)$ where $b = k_p$ and $c = k_d$. Solving for $\phi(t)$ with Wolfram Mathematica, with $\phi(0) = \dot{\phi}(0) = 0$, and discarding transient terms, we obtain the steady-state value of the amplitude a

$$\bar{a} = \frac{\alpha\omega\left(k_d I\omega^2 - bk_d + bc\right)}{\left(I\omega^2 - b\right)^2 + c^2\omega^2}. \tag{9}$$

Substituting (7) and (9) into (6) and defining $\bar{\phi} = \bar{a}\sin(\omega t)$ and $Y = \dot{y}$, the previous arguments suggest that the y-component of the CM velocity approximately takes the form:

$$\dot{Y}\left(t\right) = f_x\left(t\right) - f_y\left(t\right)Y\left(t\right) \tag{10}$$

$$\begin{cases} f_x\left(t\right) = C_1\bar{a}\omega\sin\bar{\phi}\cos\bar{\phi}\sin\left(\omega t + \frac{\bar{\delta}}{2}\right) \\ f_y\left(t\right) = C_2\sin^2\bar{\phi} \end{cases} \tag{11}$$

where C_1 and C_2 are constants that absorb L, m, and c_n, and account for the relative contributions of propulsive and breaking forces. For low-acceleration, low-amplitude locomotion, the $O(N)$ second-order differential equations needed to describe the motion of the snake's links can thus be approximated by a single first-order differential equation. A similar conclusion was reached in [5] by modeling a snake as a serial linkage of prismatic joints and averaging over an oscillation period. Equation (11) illustrates that period-averaged propulsive forces in serpentine locomotion arise from the phase offset between the lateral motion of a link and its orientation.

The $\dot{y}(t)$ curve output by (10) was compared at fixed design parameters to the results of a detailed MBD model, described in [18], in which the snake is treated as a serial linkage of constant mass density links joined by revolute joints. Equation (10) was solved for Y with the ode45 numerical solver in MATLAB over a 30-s interval, where the robot starts from rest and has model parameters $N = 3$, $L = 2$, $m = 1$, $I = mL^2/12$, $c_n = 1$, $c_t = 0$, and $k_p = k_d = 12.5$. The tunable parameters were set to values of $C_1 = 35.4$, $C_2 = 25$, $b = 0.52$, and $c = 0.30$. At these fixed values of the design parameters, the model in (10) and (11) is able to accurately reproduce the effects of changing α and ω, with less than 1% error in the predicted values of $\bar{a}$ for $\omega >$ 10 Hz. The situation worsens for small ω, with approximately 40% error for $\omega = 2$ Hz. A comparison of the forward speeds predicted by the two models is displayed in Fig. 3 for $\alpha = \{0.5, 1\}$ rad and $\omega = \{2, 5, 10, 20\}$ Hz. By (9), the assumption of small a is equivalent, to first order in ω, to the assumption of small α / ω. At $\alpha = 0.5$, for all computed values of ω, the model predictions of forward speed at the end of the 30-s

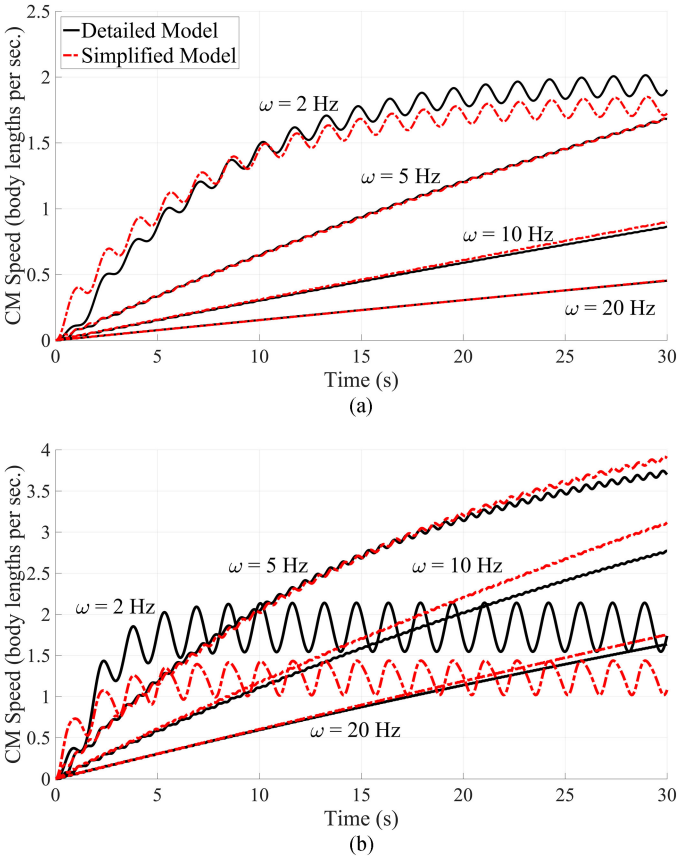

Fig. 3. Comparison of the full multibody dynamic model (black) with the single-body model (light) at various oscillation frequencies for (a) α = 0.5 rad and (b) α = 1 rad.

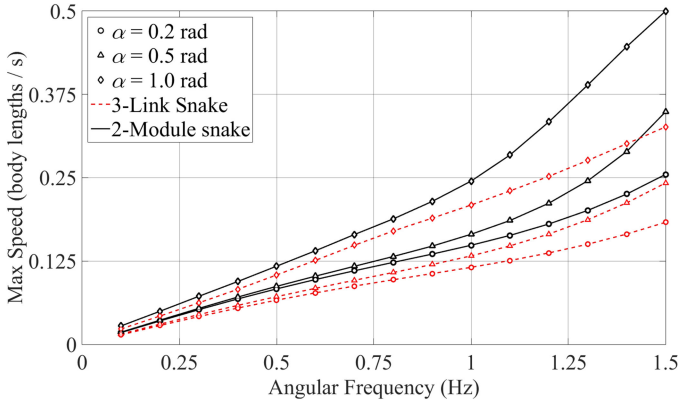

Fig. 4. Simulated steady-state speeds of two 2-DOF snake robots, with three links (dotted line) and seven (solid line), as *a* and ω are varied.

interval differ by no more than 8.2% and the amplitudes of the oscillations about this value differ by no more than 7.8%. At $\alpha = 1$, the predictions of the single-body model worsen, with speed and amplitude errors reaching approximately 29.8% and 33.3%, respectively, at $\omega = 2$ Hz. (At $\alpha = 1$ rad and $\omega = 2$ Hz, $\bar{a} = 1$ rad, and the small-amplitude assumption is violated.)

IV. Control

We begin this section with a discussion of optimizing kinematic constraints in a snake robot composed of coupled linkages. We then introduce a controller for this case and perform a feedback linearization of the motor-pulley dynamics. Finally, we describe how the spring-cable system described in Section II-B can be used to interact with objects.

A. Lateral Undulation in a Snake Robot With Coupled Joints

As discussed in Section III-A, a snake robot performing lateral undulation forms a discrete approximation to a sinusoid, and the snake's locomotive efficiency depends on the closeness of this fit. Since the kinematic constraints are fixed, the closeness of the fit will decrease if the wave's amplitude or wavelength are varied. Fitting a convex section of sine from above or below with a convex polygonal linkage, it follows from the triangle inequality that the fit's accuracy can always be improved by doubling the number of links.[2]

To construct a snake composed of coupled linkages, we replace each pair of links of length L in an uncoupled snake with a linkage. Optimal pulley radii are determined by fitting the linkage to the section of the sine wave approximated by the old link-pair, of amplitude $L\cos(\bar{\alpha}/2)$ and wavelength $4L\sin(\bar{\alpha}/2)$, where $\bar{\alpha}$ is the maximum angular displacement in the uncoupled snake. We fit at maximum angular displacement since the linkage's fit worsens more quickly with increasing α. Maximum angular displacement was chosen in our prototype as $\bar{\alpha} = \pi/2$, a reasonable value since locomotive efficiency decreases as α approaches π. The linkage was fit by minimizing the summed distances of the link centers to a sine wave with the above-mentioned parameters and an arc length equal to the linkage length.

By analogy with (4), a snake robot composed of *i* coupled linkages described by (1) can fit a sinusoid by oscillating the weighted sum of each linkage's interior angles sinusoidally

$$\tau_{M,i} = k_p \left(\theta_{\mathrm{ref},i} - \sum_{j=1}^{N-1} c_j \theta_{ij} \right) + k_d \left(\dot{\theta}_{\mathrm{ref},i} - \sum_{j=1}^{N-1} c_j \dot{\theta}_{ij} \right) \tag{12}$$

where N is the number of links in each coupled linkage, k_p and k_d are, respectively, proportional and derivative gains, θ_{ij} is the *i*th linkage's *j*th joint angle, $\theta_{\mathrm{ref},i}$ is given by (4), and $c_j = (r_j - r_{j-1})/r_{N-1}$ weights the joints by their angular displacements, where r_j is the *j*th pulley radius [18]. The summations in (12) are discrete measures of the linkage's average curvature and its derivative. In the case of zero spring-extension, (12) amounts to a sinusoidal oscillation of the pulley.

Using the MBD model of [18], we tested the effect of increased articulation in a two-DOF snake by comparing the steady-state speed of a three-link snake with a snake composed of two, four-link linkages. The two simulated snakes were of equal body length and both applied (12), with identical control parameters. The results of these simulations, displayed in Fig. 4,

[2]See: https://github.com/RM-Lab/Robosnake/blob/master/Supplements.pdf

indicate that the more highly articulated snake outperforms the three-link snake across all tested control parameters.

B. Pulley Feedback Linearization

As discussed in Section III-A, an N-link snake robot moving in the xy-plane can be modeled as a serial chain of straight links joined by revolute joints, which can be described by a system of $3N$ second-order differential equations and $2(N–1)$ algebraic constraints. The global position of the ith link CM is specified by a vector of generalized coordinates $\mathbf{q}_i = [\mathbf{r}_i\ \phi_i]^T$, where $\mathbf{r}_i = [x_i\ y_i]$ is the global position of the ith link and ϕ_i is its global orientation. We also define, for the ith link, a vector of Lagrange multipliers $\lambda_i = [\lambda_{x,i}\ \lambda_{y,i}]^T$, a diagonal 3×3 generalized mass matrix $\mathbf{M}_i$, a generalized external force vector $\mathbf{F}_{\text{ext},i}$, and a vector of generalized actuation forces $\mathbf{U}_i = [0\,0\,U_i]^T$, calculated from the output τ_M of (12), by way of the cable equations in (2).

The differential algebraic equations for the system may be written in the form

$$\begin{cases} \mathbf{M}_i\ddot{\mathbf{q}}_i = \mathbf{F}_{\text{ext},i} + \mathbf{f}\left(\phi_i, \lambda_i, \lambda_{i-1}\right) + \mathbf{U}_i \\ \mathbf{r}_j - \mathbf{r}_{j+1} = \mathbf{g}\left(\phi_j, \phi_{j+1}\right) \end{cases}. \tag{13}$$

($i \in [1, N]$ and $j \in [1, N-1]$), where $\mathbf{f}$ and $\mathbf{g}$ are vector valued functions that account for the mechanism's internal forces [28].

Using (2), the angular acceleration of the motor/pulley can be related to the joint torque τ_i as $I_M\ddot{\theta}_M = \bar{\tau}_M + I\sum_{i=1}^{N-1}\beta_i\tau_i$, where I is the link moment of inertia, I_M is the effective mass moment of inertia of the motor-pulley system, $\theta_M = \theta_P$ is motor/pulley angular displacement, $\bar{\tau}_M$ is the applied motor torque, and $\beta_i = \frac{1}{R}(r_i - r_{i-1})$. The joint dynamics may be written as $I\ddot{\theta}_i = \tau_i + T_i$, where T_i is the ith angular component of $\mathbf{F}_{\text{ext},i} + \mathbf{f}(\phi_i, \lambda_i, \lambda_{i-1})$ in (13), and where the λ_i are given, in terms of the actuation and frictional forces and the generalized coordinates and their derivatives, by a system of $4N - 2$ equations. The motor-pulley dynamics may then be written as

$$I_M\ddot{\theta}_M = \bar{\tau}_M + I\sum_{i=1}^{N-1}\beta_i\left(I\ddot{\theta}_i - T_i\right). \tag{14}$$

Defining τ_{NL} as the second summation in (14) and setting a motor torque of $\bar{\tau}_M = \tau_M - \tau_{NL}$, where τ_M is given by (12), (14) becomes $\tau_M = I_M\ddot{\theta}_M - I\sum_{i=1}^{N-1}\beta_i\ddot{\theta}_i$. Assuming zero spring displacement, θ_i may be written in terms of θ_M using (1), giving

$$\left(I_M - I\sum_{i=1}^{N-1}{\beta_i}^2\right)\ddot{\theta}_M = \tau_M. \tag{15}$$

Thus, the linear joint relation in (1) due to the circular cable routing allows for a feedback linearization of the pulley dynamics. This method was tested in simulation in a snake robot composed of two four-link modules where estimates of the external forces were input to the $\mathbf{F}_{\text{ext},i}$ and λ_i, at various values of α and ω. In simulation, replacing τ_M with $\bar{\tau}_M$ monotonically increased the snake robot's steady-state speed as estimates of external forces were varied from 0% to 100% of the true values, increasing between 15.5% and 27.5% for perfect estimates, as shown in Fig. 5.

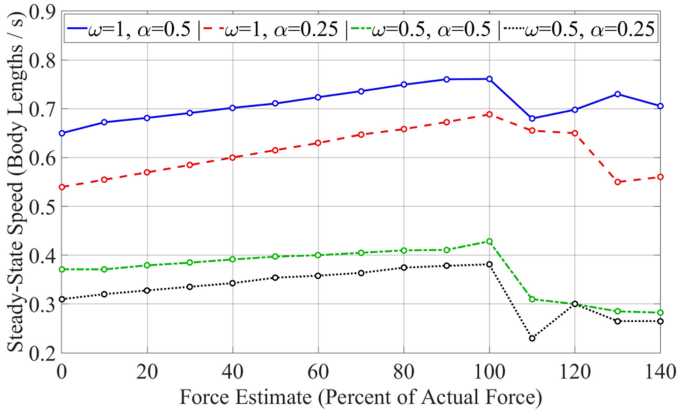

Fig. 5. Steady-state speed for a two-module snake robot applying pulley feedback linearization as estimates of external forces are varied between 0% and 140% of the actual values.

C. Path Following in the Presence of Obstacles

Thanks to the cable-aligned springs, external forces acting on the snake robot may be detected using Hooke's Law by measuring the forced angular displacements of the joints. The curvature of the snake robot is then controlled by adding an offset $\theta_{\text{obs}} = -k_{\text{obs}}\sum_{i=1}^{N_b-1} c_i e_i$ to θ_0, where k_{obs} is a gain that determines the direction and extent of the curvature, c_i is the joint weighting defined in Section IV-A, and e_i is the obstacle induced angular displacement in the ith joint. Here, e_i is computed by comparing the measurements of the rotary position sensors with the joint angles given by the kinematic constraints in (1). The above-mentioned definition is an application to a coupled linkage of the principle outlined in [29] and [30], where a snake robot is able to slide around obstacles by applying a torque proportional to a power of obstacle-induced curvature. Notice that this definition of θ_{obs} also results in an equivalent spring force between the snake and obstacle.

Adaptively steering using the above-mentioned procedure results in a difficult to predict change in the snake's heading, which is dependent on obstacle shape and size and the angle of attack. We, therefore, run the obstacle interaction procedure in parallel with a path following scheme by defining $\theta_0 = \theta_h + \theta_{\text{obs}}$, where, inspired by, e.g., [31]–[33], we set $\theta_h = A_h(\phi_h - \phi_{\text{ref}})$. Here, A_h is a gain, $\phi_h = \frac{1}{N}\sum_{i=1}^{N}\phi_i$ is the snake's heading, and $\phi_{\text{ref}} = \phi_p - \arctan[P_h P_X + I_h \arctan(\int_0^t P_X\,dt')]$ is a reference heading. In the expression for ϕ_{ref}, ϕ_p is the global orientation of the desired path, P_X is the signed distance of the robot CM perpendicular to the desired path, and P_h and I_h are proportional and integral heading gains. The integral component in ϕ_{ref} is necessary only to compensate for constant disturbances (e.g., water currents, gravitational forces on a slope, etc.), whereas local disturbances can be handled by the proportional term. Setting $P_h = p_1 + \arctan^2(p_2\ \phi_{AoA})$, where p_1 and p_2 are gains and ϕ_{AoA} is the angle of attack, the robot can be made to more aggressively approach the desired path when the heading error

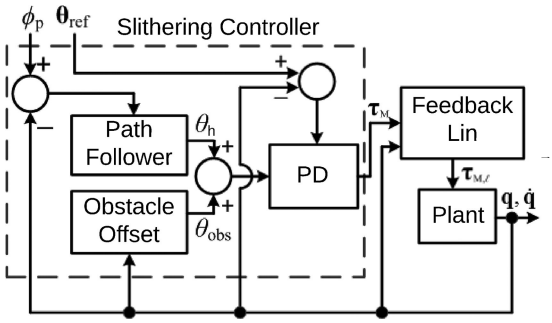

Fig. 6. Complete control scheme for the cable-driven snake robot.

is large (I_h can be defined in the same way). A block diagram of the full control algorithm for the snake robot is displayed in Fig. 6.

V. Experiments

This section presents experimental studies of force control, locomotion, and adaptation to obstacles, using the snake robot prototype introduced in Section II.

A. Force Control

Under the assumption of static equilibrium, and assuming the base of a linkage is fixed with respect to an external object, the torque acting on each joint is related to its angular displacement by a simple application of Hooke's Law. The joint torques $\tau = [\tau_i \dots \tau_{N-1}]^T$ can then be written in terms of the net force $F_e = [F_{ex}, F_{ey}]^T$ applied by the end effector (the last link of the linkage) as $\tau = J^T R_{0e}^T F_e$ where $\mathbf{J}$ is the linkage's Jacobian and R_{0e} is the rotation matrix from the base frame to the end effector frame. Multiplying by the pseudoinverse of J^T, the end-effector force can be written in terms of the joint torques as $F_e = R_{0e} J^{T\dagger} \tau$, where τ is given in terms of the pulley angular displacement $\Delta\theta_P$ by (1). Numerically solving the two resulting transcendental equations for the two components of $\mathbf{F}_e$, $\Delta\theta_P$ can be written as a function of F_x or F_y, only one of which can be controlled by a 1-DOF linkage. Fortunately, controlling $F_{e,x}$ is sufficient for pushing off of or grasping external objects.

The mechanism's ability to control $F_{e,x}$ using a PD controller on $\Delta\theta_P$ was tested experimentally, in two configurations, $\theta_1 = 0°$ and $\theta_1 = 30°$, for three desired force outputs, 10, 15, and 20 N. A single linkage was placed horizontally so that gravitational effects could be ignored, and allowed to reach the desired configuration unimpeded. The end effector was then placed parallel to an MLP-25 compression load cell rated for 44.5 N, and the base of the linkage was fixed to ground. In practice, $\Delta\theta_P$ had to be adjusted about 6% above the computed value in order to achieve the desired force output, possibly as a result of frictional effects or errors in the kinematic constraints. As predicted, in the $\theta_1 = 30°$ configuration, equal end-effector forces require $\Delta\theta_P$ values approximately 1.4 times the values required for the $\theta_1 = 0°$ case.

The results of these experiments are shown in Fig. 7, after application of a locally weighted linear regression smoothing. Note that the load cell used in these experiments has a settling

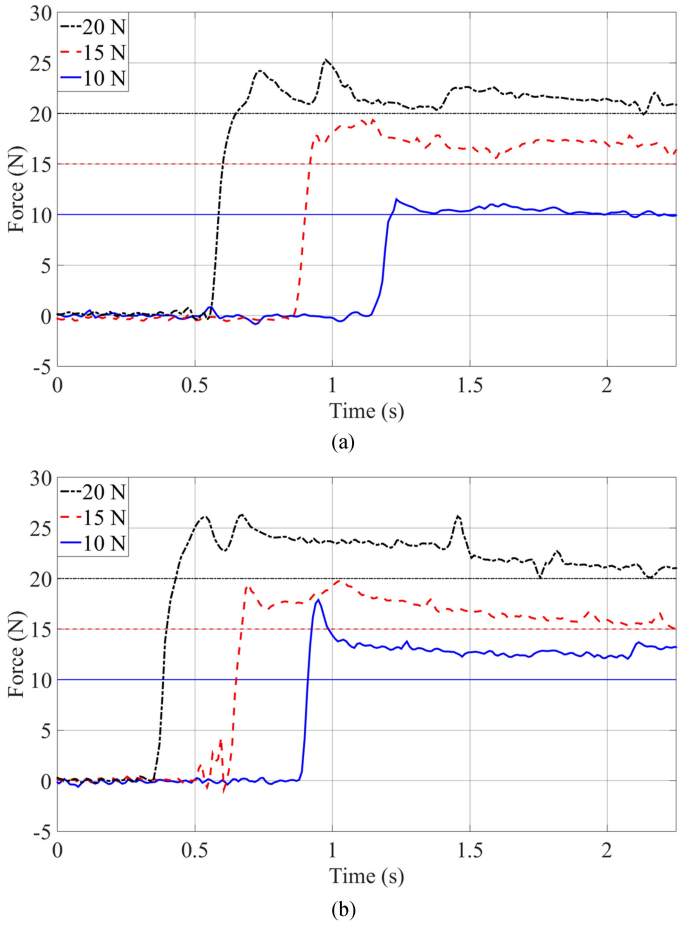

Fig. 7. Force control experiments for (a) straight configuration ($\theta_1 = 0°$) and (b) curved configuration ($\theta_1 = 30°$).

time of over a second, which causes the force measurements to decrease slightly after the applied torque has plateaued. The results in Fig. 7 demonstrate that the linkage is able to successfully control the perpendicular component of the end-effector force by controlling the pulley's angular position, with less than 5% error in all but one of the six trials.

B. Locomotion and Steering

As discussed in [18], the controller outlined in Fig. 6 was tested in simulation using the MBD model from Section IV. In the prototype, the feedback linearization was removed, the path follower was replaced by manual steering, and the controller output was cascaded into the servomotor's PID loop.

Planar locomotion and steering were tested in the prototype by tracking its trajectory on floor tiles over roughly four periods of oscillation, starting from a straight configuration and with $\alpha = 2.45$ rad, $\delta = 1.27$ rad, and $\omega = 3.77$ Hz. The front link of the snake was labeled with a blue marker and the back link with a red marker, as shown in Fig. 8.

A 12.3-megapixel camera facing directly down at a height of about two meters was used to record the snake motion.

These videos were sampled at 10 Hz and scaled using the known dimensions of the tiles, after which the centroids of each

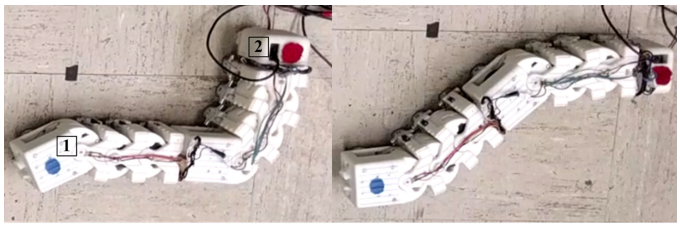

Fig. 8. Snapshots of the snake robot executing a counterclockwise turn, showing a half-period of oscillation between (a) and (b). The front link is marked by (1) and the control module is marked by (2).

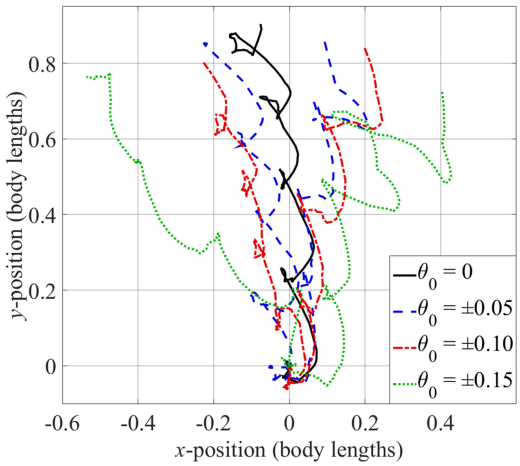

Fig. 9. Trajectories of the front link of the robot over four oscillation periods for various values of θ_0. (Positive values correspond to clockwise turning.)

marker were tracked. The resulting trajectories are shown in Fig. 9, for values of θ_0 between –0.15 rad and 0.15 rad.

The prototype can travel at a maximum speed of about 0.07 body lengths per second (BL/s), comparable to the maximum speed of the 7-DOF Amphibot (also at 0.07 BL/s), but several times slower than the 19-DOF ACM-RIII (at about 0.25 BL/s) [34]. The prototype appears to have a slight bias to the left and exhibits higher amplitude oscillations during right turning than left turning, most likely on account of asymmetries in the cable constraints.

C. Obstacle Interaction

The obstacle interaction procedure in Section IV-C was tested experimentally for three values of k_{obs} by recording the trajectory of the snake robot as it moved past a circular, 5-kg cast iron plate, with a radius of 8 cm. The robot was started in a straight configuration, oriented 45° from the global y-axis, flush with the obstacle and tangent to it. The robot was then commanded to move forward, with $\theta_0 = 0$ and the other control parameters set as in Section V-B. The front and back of the snake were tracked and the angle that the vector between them formed with the global y-axis was taken as the snake's heading. With $k_{\text{obs}} = 0$, the snake can be observed to rotate about the obstacle by the following process. The front module first contacts the obstacle and induces a moment about the snake's CM that rotates the robot away from the obstacle. However, this movement brings the back module into contact with the obstacle, and a moment is then induced in the opposite direction. The front module eventually moves past the obstacle and only the back module continues to contact it. The snake is then progressively rotated, but the curvature of its trajectory is low enough that the point of contact with the obstacle moves down the length of the back module until the snake eventually loses contact with the obstacle and moves past it. Thus, two competing tendencies determine the amount of rotation induced by an obstacle: the magnitude of the moment produced by each impact and the amount by which the point of contact moves down the length of the snake between impacts.

In the experiment, the case $k_{\text{obs}} = 0$ resulted in about a 168° change in orientation toward the obstacle. Increasing k_{obs} to 1.33, the snake curved more in the direction of contact, resulting in an orientation change of about 221° over the same period. On the other hand, negative values of k_{obs} offset obstacle induced rotation by rotating the reference heading in the opposite direction, as in the case $k_{\text{obs}} = -2$, where the snake curved away from the obstacle with a 17° change to its initial heading.

VI. Conclusion

This paper presented the development of a cable-driven snake robot with coupled joints, which incorporates elastic elements as a means of producing both passive and controlled adaptation to obstacles. A simplified model of serpentine locomotion was developed and used to analyze how the propulsive force produced by a snake robot is related to the number of links it contains. A control scheme was devised for a snake robot comprised of coupled linkages and combined with an obstacle interaction scheme and path follower. These ideas were tested in simulation and experiments with a prototype.

As a hybrid of traditional direct-drive serpentine mechanisms and externally actuated snakelike manipulators, the self-contained cable-actuated mechanism presented in this paper represents an alternative approach to snake robot design. Actuating multiple joints simultaneously via circularly routed antagonistic cable pairs is a promising approach to lowering the weight and size of mobile snake robots, and offers significant prospects for further miniaturization. With more sophisticated cable routing schemes, the use of multiple multiradius pulleys may also allow for three-dimensional coupled bending in a single module, enabling more natural and versatile locomotion.

References

[1] S. Hirose, *Biologically Inspired Robots (Snake-Like Locomotors and Manipulators)*. Oxford, U.K.: Oxford Univ. Press, 1993.
[2] P. Liljebäck, K. Pettersen, Ø. Stavdahl, and J. Gravdahl, "Fundamental properties of snake robot locomotion," in *Proc. IEEE/RSJ Int. Conf. Intell. Robot. Syst.*, Taipei, Taiwan, 2010, pp. 2876–2883.
[3] J. Gray, "The mechanism of locomotion in snakes," *J. Exp. Biol.*, vol. 23, no. 2, pp. 101–120, 1946.
[4] D. Hu, J. Nirody, T. Scott, and M. Shelley, "The mechanics of slithering locomotion," *Proc. Nat. Acad. Sci.*, vol. 106, no. 25, pp. 10081–10085, 2009.
[5] P. Liljebäck, K. Pettersen, Ø. Stavdahl, and J. Gravdahl, *Snake Robots: Modeling, Mechatronics, and Control*. London, U.K.: Springer, 2013.

[6] A. Degani, H. Choset, B. Zubiate, T. Ota, and M. Zenati, "Highly articulated robotic probe for minimally invasive surgery," in *Proc. IEEE Eng. Med. Biol. Soc.*, 2006, vol. 2006, pp. 4167–4172.
[7] J. Burgner-Kahrs, D. Rucker, and H. Choset, "Continuum robots for medical applications: A survey," *IEEE Trans. Robot.*, vol. 31, no. 6, pp. 1261–1280, Dec. 2015.
[8] A. Transeth, K. Pettersen, and P. Liljebäck, "A survey on snake robot modeling and locomotion," *Robotica*, vol. 27, no. 7, p. 999–1015, 2009.
[9] S. Hirose and H. Yamada, "Snake-like robots: Machine design of biologically inspired robots," *IEEE Robot. Autom. Mag.*, vol. 16, no. 1, pp. 88–98, Mar. 2009.
[10] C. Wright *et al.*, "Design and architecture of the unified modular snake robot," in *Proc. IEEE Int. Conf. Robot. Autom.*, 2012, pp. 4347–4354.
[11] D. Rollinson, A. Buchan, and H. Choset, "Virtual chassis for snake robots: Definition and applications," *Adv. Robot.*, vol. 26, no. 17, pp. 2043–2064, 2012.
[12] S. Takaoka, H. Yamada, and S. Hirose, "Snake-like active wheel robot ACM-R4.1 with joint torque sensor and limiter," in *Proc. IEEE Int. Conf. Intell. Robot. Syst.*, 2011, pp. 1081–1086.
[13] G. Granosik, M. G. Hansen, and J. Borenstein, "The OmniTread serpentine robot for industrial inspection and surveillance," *Ind. Robot Int. J.*, vol. 32, no. 2, pp. 139–148, 2005.
[14] S. Murata, E. Yoshida, A. Kamimura, H. Kurokawa, K. Tomita, and S. Kokaji, "M-TRAN : Self-reconfigurable modular robotic system," *Trans. Mech.*, vol. 7, no. 4, pp. 431–441, 2002.
[15] M. Yim, D. Duff, and K. Roufas, "PolyBot: A modular reconfigurable robot," in *Proc. IEEE Int. Conf. Robot. Autom.*, 2000, vol. 1. pp. 514–520.
[16] B. Ouyang, Y. Liu, and D. Sun, "Design of a three-segment continuum robot for minimally invasive surgery," *Robot. Biomimetics*, vol. 3, no. 1, pp. 1–4, 2016.
[17] P. Racioppo, W. Saab, and P. Ben-Tzvi, "Design and analysis of a reduced degree of freedom modular snake robot," in *Proc. Int. Des. Eng. Tech. Conf. Comput. Inf. Eng. Conf.*, 2017, paper DETC2017-67377.
[18] P. Racioppo and P. Ben-Tzvi, "Modeling and control of a cable driven modular snake robot," in *Proc. IEEE Conf. Control Technol. Appl.*, 2017, pp. 468–473.
[19] W. S. Rone and P. Ben-Tzvi, "Mechanics modeling of multisegment rod-driven continuum robots," *J. Mech. Robot.*, vol. 6, no. 4, 2014, Art. no. 41006.
[20] W. S. Rone and P. Ben-Tzvi, "Continuum robot dynamics utilizing the principle of virtual power," *IEEE Trans. Robot.*, vol. 30, no. 1, pp. 275–287, Feb. 2014.
[21] W. Saab and P. Ben-Tzvi, "Design and analysis of a discrete modular serpentine robotic tail for improved performance of mobile robots," in *Proc. ASME Int. Des. Eng. Tech. Conf. Comput. Inf. Eng. Conf.*, 2016, paper DETC2016-59387.
[22] G. Pratt and M. Williamson, "Series elastic actuators," in *Proc. IEEE/RSJ Int. Conf. Intell. Robot. Syst.*, 1995, pp. 399–406.
[23] D. Rollinson, S. Ford, B. Brown, and H. Choset, "Design and modeling of a series elastic element for snake robots," in *Proc. ASME Dyn. Syst. Control Conf.*, 2013, paper DSCC2013-3875.
[24] D. Rollinson *et al.*, "Design and architecture of a series elastic snake robot," in *Proc. IEEE/RSJ Int. Conf. Intell. Robot. Syst.*, 2014, pp. 4630–4636.
[25] S. Ma, "Analysis of snake movement forms for realization of snake-like robots," in *Proc. IEEE Int. Conf. Robot. Autom.*, 1999, vol. 4, pp. 3007–3013.
[26] M. Saito, M. Fukaya, and T. Iwasaki, "Serpentine locomotion with robotic snakes," *IEEE Control Syst. Mag.*, vol. 22, no. 1, pp. 64–81, Feb. 2002.
[27] P. Liljeback, K. Pettersen, Ø. Stavdahl, and J. Gravdahl, "Controllability and stability analysis of planar snake robot locomotion," *IEEE Trans. Autom. Control*, vol. 56, no. 6, pp. 1365–1380, Jun. 2011.
[28] E. Haug, *Computer-Aided Kinematics and Dynamics of Mechanical Systems, Volume I: Basic Methods*. Boston, MA, USA: Allyn and Bacon, 1989.
[29] P. Liljebäck, I. Haugstuen, and K. Pettersen, "Path following control of planar snake robots using a cascaded approach," in *Proc. 49th IEEE Conf. Decis. Control*, 2010, pp. 1969–1976.
[30] P. Liljebäck and K. Pettersen, "Waypoint guidance control of snake robots," in *Proc. IEEE Int. Conf. Robot. Autom.*, 2011, vol. 7491, pp. 937–944.
[31] T. Fossen, *Marine Control Systems: Guidance, Navigation and Control of Ships, Rigs and Underwater Vehicles*. Trondheim, Norway: Springer, 2002.
[32] H. Date and Y. Takita, "Adaptive locomotion of a snake like robot based on curvature derivatives," in *Proc. Int. Conf. Intell. Robots Syst.*, 2007, pp. 3554–3559.
[33] D. Rollinson, K. Alwala, N. Zevallos, and H. Choset, "Torque control strategies for snake robots," in *Proc. IEEE Int. Conf. Intell. Robot. Syst.*, 2014, pp. 1093–1099.
[34] J. Hopkins, B. Spranklin, and S. Gupta, "A survey of snake-inspired robot designs," *Bioinspiration Biomimetics*, vol. 4 no. 2, 2009, Art. no. 021001.

Peter Racioppo (S'16) received the B.S. degree in physics from the University of California, Los Angeles, Los Angeles, CA, USA, in 2014, and the M.S. degree in mechanical engineering from Virginia Tech, Blacksburg, VA, USA, in 2018.

His current research interests include dynamical systems and control, robotics and mechatronics, motion planning, and control of multiagent systems.

Pinhas Ben-Tzvi (S'02–M'08–SM'12) received the B.S. (*summa cum laude*) degree in mechanical engineering from the Technion—Israel Institute of Technology, Haifa, Israel, in 2000, and the M.S. and Ph.D. degrees in mechanical engineering from the University of Toronto, Toronto, ON, Canada, in 2002 and 2008, respectively.

He is currently an Associate Professor in mechanical engineering and electrical and computer engineering, and the founding Director of the Robotics and Mechatronics Laboratory, Virginia Tech, Blacksburg, VA, USA. His current research interests include robotics and intelligent autonomous systems, mechatronics, human–robot interactions, dynamic systems and control, mechanism design and system integration, and novel sensing and actuation.

Dr. Ben-Tzvi is the recipient of the 2018 Virginia Tech Faculty Fellow Award, the 2013 GW SEAS Outstanding Young Researcher Award, and Outstanding Young Teacher Award, and other honors and awards. He is the Technical Editor for the IEEE/ASME TRANSACTIONS ON MECHATRONICS, Associate Editor for *ASME Journal of Mechanisms and Robotics*, Associate Editor for IEEE ROBOTICS AND AUTOMATION MAGAZINE, and an Associate Editor for the *International Journal of Control, Automation and Systems* and served as an Associate Editor for IEEE ICRA 2013–2018. He is a member of the ASME.